Research Article | Vol. 29, No. 23 / 8 Nov 2021 / Optics Express 38119
Optics EXPRESS

Bright, single helicity, high harmonics driven by mid-infrared bicircular laser fields

KEVIN M. DORNEY,[1,2,5,*] TINGTING FAN,[1,5] QUYNH L. D. NGUYEN,[1,5] JENNIFER L. ELLIS,[1] DANIEL D. HICKSTEIN,[1] NATHAN BROOKS,[1] DMITRIY ZUSIN,[1] CHRISTIAN GENTRY,[1] CARLOS HERNÁNDEZ-GARCÍA,[3] HENRY C. KAPTEYN,[1,4] AND MARGARET M. MURNANE[1]

[1]JILA - Department of Physics, University of Colorado Boulder and NIST, Boulder, CO 80309, USA
[2]Current address: imec, Kapeldreef 75, 3000 Leuven, Belgium
[3]Grupo de Investigación en Aplicaciones del Láser y Fotónica, University of Salamanca, E-37008 Salamanca, Spain
[4]KM Laboratories, Inc., 4775 Walnut St., Boulder, CO 80301, USA
[5]These authors contributed equally
*kevin.dorney@colorado.edu

Abstract: High-harmonic generation (HHG) is a unique tabletop light source with femtosecond-to-attosecond pulse duration and tailorable polarization and beam shape. Here, we use counter-rotating femtosecond laser pulses of 0.8 μm and 2.0 μm to extend the photon energy range of circularly polarized high-harmonics and also generate single-helicity HHG spectra. By driving HHG in helium, we produce circularly polarized soft x-ray harmonics beyond 170 eV—the highest photon energy of circularly polarized HHG achieved to date. In an Ar medium, dense spectra at photon energies well beyond the Cooper minimum are generated, with regions composed of a single helicity—consistent with the generation of a train of circularly polarized attosecond pulses. Finally, we show theoretically that circularly polarized HHG photon energies can extend beyond the carbon K edge, extending the range of molecular and materials systems that can be accessed using dynamic HHG chiral spectro-microscopies.

1. Introduction

High harmonic generation (HHG) is the most extreme nonlinear optical process observed to date, [1,2,3] upconverting femtosecond laser light into short-wavelength high harmonics that can span >5000 orders [4]. When optimally phase matched, [4,5,6,7,8,9] HHG is a robust tabletop-scale source of bright, coherent, extreme ultraviolet (EUV) and soft X-ray (SXR) beams, [10,11] with pulse durations in the femtosecond and attosecond range [12,13,14,15] that can capture the fastest charge, spin, and phonon interactions in molecules and materials [16,17,18,19,20]. Moreover, the high spatial and temporal coherence of HHG sources has enabled powerful new capabilities in nanoscale functional imaging [21,22,23,24,25,26].

In HHG in gases, an electron wavepacket is liberated from the ground state of an atom, then accelerated by the laser field, before recombining with the parent ion via a radiative dipole transition from laser-dressed continuum states back to the ground state [3,27,28]. As a result, the properties of the emitted HHG radiation are exquisitely sensitive to the driving laser field [29] and the electronic structure of the HHG medium. These principles have been successfully exploited to tailor the spectral, temporal, spatial, and polarization properties of high harmonics, enabling the generation of circularly polarized EUV/SXR radiation [30,31,32,33,34], high-harmonics with unique spatial angular momentum structure [35,36,37], single attosecond pulses [13,15,28,38], and bright phase-matched high-harmonics spanning from EUV to keV photon energies [4,5,7,11,12].

#440813 https://doi.org/10.1364/OE.440813
Journal © 2021 Received 17 Aug 2021; revised 17 Oct 2021; accepted 20 Oct 2021; published 1 Nov 2021

Optics EXPRESS

In particular, when HHG is driven by a "bicircular" laser field composed of two circularly polarized, counter-rotating laser fields (bicircular) [39,40], selection rules for the conservation of spin angular momentum lead to the emission of pairs of harmonics, each with left and right circular polarization. Initial works used a bichromatic laser field composed of a fundamental laser (ω_1) field and its second harmonic (ω_2=2ω_1), which results in a characteristic three-fold symmetric driving laser field [31,41]. This results in good phase matching and bright HHG emission, [31,32] since the shape of the driving laser field remains constant with propagation—in contrast to driving HHG with a linearly-polarized bichromatic field. Moreover, by adjusting the relative intensity of the individual laser fields, the ellipticity of the underlying attosecond bursts can be controlled [42,43], providing elliptically polarized EUV waveforms for spectroscopy of chiral systems [44,45,46]. However, the bright HHG photon energy cutoff is reduced compared to linearly polarized fields. Pushing beyond these limits involves the use of optimized phase-matched geometries with long interaction lengths, as well as using longer wavelength lasers in the mid-infrared (MIR). For instance, Fan and coworkers showed that BHHG driven by non-commensurate 0.8 μm and 1.3 μm lasers leads to emission of elliptical high-harmonics in the SXR region, which enabled x-ray magnetic circular dichroism (XMCD) measurements at the Gd *N* edge (~145 eV) [32].

In this work, we demonstrate that high harmonics driven by bicircular MIR laser fields can exhibit a photon energy cutoff that extends well into the SXR region. By driving high harmonics from He in a waveguide geometry with bicircular laser fields of 0.8 μm and 1.3 μm, we generate bright, highly elliptically polarized high-harmonic spectra up to 170 eV. This photon energy range spans many of the *N* absorption edges of rare-earth ferrimagnetic materials (e.g., Gd, Tb, Dy), enabling new regimes of magnetic spectroscopies from table-top sources. We also reveal new physics in the vicinity of the Cooper minimum electronic resonance in Argon gas: with optimal phase matching, an HHG spectrum composed of a single helicity is obtained beyond the Cooper minimum in Ar, spanning the *M* edges of many *3d* magnetic materials. In previous work, circularly-polarized HHG spectra generated in Ar exhibit a characteristic helicity reversal near the Cooper minimum [45,47] (as also observed in this work), but harmonics of both helicities were still present after the Cooper minimum. Here we utilize a phase-matched waveguide geometry to exploit this reversal and, for the first time, synthesize a high-harmonic spectrum composed of a single helicity. These results clearly demonstrate the advantages of employing bicircular fields with MIR components, while also providing unique light sources capable of probing chiral and electronic dynamics in materials, nano and molecular systems.

2. Experimental and theoretical methods

2.1. Experimental methods

In our experiment, circularly polarized high harmonics are generated in He, Ne, or Ar via collinear mixing of circularly polarized near-infrared (NIR) (0.8 μm, 45 fs, right circularly polarized (RCP)) and MIR laser fields (1.3 or 2.0 μm, left circularly polarized (LCP)) in a hollow-core, gas-filled capillary waveguide (see Fig. 1).

Approximately 90% of the output of a single-stage Ti:sapphire laser amplifier (9 mJ, 45 fs, 1 kHz, KMLabs Inc.) is sent into a home-built three-stage optical parametric amplifier (OPA) [48] to generate the MIR driving field, while the residual 10% of the output is utilized for the NIR driving field. The signal (1.3 μm, 45 fs, 1.7 mJ) and idler waves (2.0 μm, 50 fs, 0.9 mJ) are generated via nonlinear mixing in three beta-barium borate (BBO) stages in the OPA. The NIR and MIR fields are then passed through a Mach-Zhender interferometer, with waveplates (λ/2 and λ/4) inserted in each arm to produce circularly polarized beams of opposite helicity (an NIR beam of RCP and an MIR beam of LCP)). Additional waveplate-polarizer pairs are used to control the intensity prior to focusing the combined NIR (maximum coupled pulse energy of 0.4 mJ) and MIR (maximum coupled pulse energies of 1.5/0.7 mJ, for the 1.3/2.0

Optics EXPRESS

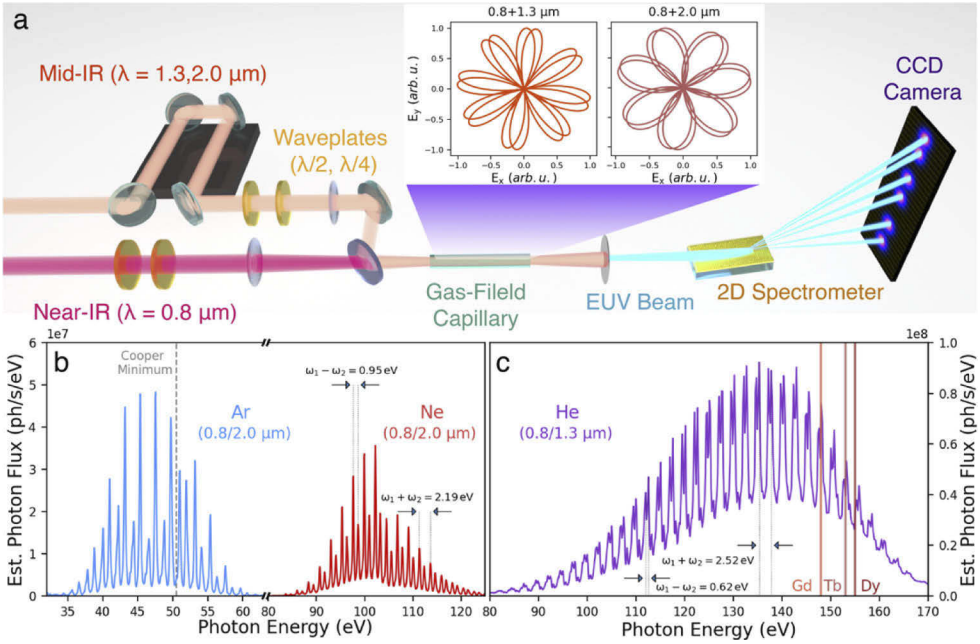

Fig. 1. (a) Experimental setup for HHG driven by a near-IR and mid-IR bicircular laser field. Highly elliptically polarized high harmonics are generated in a high-pressure hollow-core waveguide, and the emitted radiation is imaged onto a CCD camera. The inset depicts the transverse field profile of the bicircular field composed of 0.8 and 1.3/2.0 μm pulses, plotted over 2 cycles. (b) Bicircular HHG spectra produced in Ar and Ne with a 0.8 + 2.0 μm field with a backing pressure of 350 and 500 Torr, respectively (total intensities of $I_{Ar} = 9.3 \times 10^{13}\ Wcm^{-2}$ and $I_{Ne} = 1.7 \times 10^{14}\ Wcm^{-2}$) and in (c) He using a 0.8 + 1.3 μm bicircular field with a backing pressure of 600 Torr ($I_{He} = 2.3 \times 10^{14}\ Wcm^{-2}$). HHG in Ar easily extends beyond the Cooper minimum (dashed grey line), while HHG in He extends beyond the N absorption edges of $4f$ rare-earth ferromagnetic elements.

μm beams) beams into the hollow-core waveguide. For all BHHG spectra presented here, the intensity ratio of the bicircular field is set to $I_{\omega_1}/I_{\omega_2} \sim 2.0$, by adjusting the pulse energies prior to coupling into the waveguide (where I_{ω_i} is the intensity of the NIR (i=1) or MIR field (i=2)). This yields the following estimated intensities for each media: for Ar, $I_{\omega_1} = 6.1 \times 10^{13}\ Wcm^{-2}$ and $I_{\omega_2} = 3.2 \times 10^{13}\ Wcm^{-2}$ for Ne, $I_{\omega_1} = 1.1 \times 10^{14}\ Wcm^{-2}$ and $I_{\omega_2} = 6.9 \times 10^{13}\ Wcm^{-2}$, and finally for He, $I_{\omega_1} = 1.2 \times 10^{14} Wcm^{-2}$ and $I_{\omega_2} = 1.1 \times 10^{14} Wcm^{-2}$. The exit of the waveguide is directly imaged onto an X-ray CCD camera (Andor, DO940PN) via an X-ray imaging spectrometer composed of a flat grating and a pair of Kirkpatrick-Baez mirrors (Hettrick Scientific). Thin aluminum and zirconium foils are placed into the beam path before the spectrometer to reject the intense bicircular driving field and also to calibrate the spectrum. All BHHG spectra are corrected for the (theoretical) transmission of the beamline (e.g., filters, spectrometer optics, and grating efficiency) and the source flux is estimated by converting CCD counts to incident photons using the manufacturer specifications of the CCD camera.

2.2. *Theoretical simulations*

In order to gain insight into the capability of MIR sources to extend the BHHG cutoff towards the SXR region, we have performed theoretical simulations based on the Strong Field Approximation, without resorting to the saddle point approximation [29,49,50,51,52]. Note that it is known that the SFA gives better agreement, both qualitatively and quantitatively, against the solution of

Optics EXPRESS

the time dependent Schrodinger equation [53], and that in the case of the bicircular field, the complexity of the classical trajectories hinders the application of the saddle point approximation [54]. The driving field is described as a superposition of two counter-rotating circularly polarized laser pulses, with central wavelengths of λ_1 and λ_2 ($\lambda_1 > \lambda_2$). The temporal envelope of each pulse is modelled with a trapezoidal function with two cycles of linear turn-on, four cycles of constant amplitude and two cycles of linear turn-off (in terms of cycles of λ_1). The choice of a trapezoidal envelope function (as opposed to more complex pulse shapes) is to reduce the computational demand of the simulations, while still providing good agreement with experimental BHHG spectra. The electric field amplitudes of each driver have an associated intensity of $I_1 = I_2 = 2 \times 10^{14} W/cm^2$, which is commensurate with the achievable intensities from current high-intensity, table-top MIR light sources and also allows us to safely neglect effects from overionization of the He medium and other nonlinear effects.

3. Results and discussion

3.1. Generation of bright, spectrally dense, and high-energy circularly polarized high harmonics

The use of bichromatic NIR and MIR circularly-polarized driving laser fields offers unique advantages. First, the NIR-MIR bicircular fields inherently yield a dense harmonic spectral comb, which is a direct result of the spin-constrained upconversion process. Spin-conservation results in a spectrum of HHG doublets consisting of peaks with alternating helicity, separated by regions where HHG is spin-forbidden, at least for perfectly circularly polarized laser fields [32]. While we do not measure the polarization of the high harmonics in this work (which would require a well-calibrated spectrometer and polarimeter over a wide energy range), we note that the strong suppression of spin-forbidden peaks indicates that the resulting harmonics are at least highly elliptically polarized. The helicity of the harmonic peaks is easily determined by the relative helicities of the components of the bicircular field. The lower (higher) energy peak in each doublet co-rotates with the lower (higher) frequency component of the bichromatic field, while the peaks are separated by their difference in photon energy (ω_1-ω_2, Figs. 1(b)-(c)). Additionally, each peak in the doublet is separated by a neighboring doublet by the sum of the photon energies of the two drivers (ω_1+ω_2, Figs. 1(b)-(c)) [31,32,41,55,56]. This yields a high density of harmonic peaks when using NIR-MIR bicircular fields (Figs. 1(b)-(c)). Additionally, the longer wavelength of the MIR field significantly increases both the single-atom and the phase-matched cutoff photon energy. This results in SXR harmonics in He that span the N absorption edges of many $4f$ rare-earth magnetic elements (Fig. 1(c)). Meanwhile, the MIR component results in a shorter temporal-phase-matching window [5,7,14,32] that serves to broaden the harmonic peaks, which increase their spectral coverage for applications in spectroscopy or imaging.

Aside from these general characteristics of NIR/MIR bicircular-driven BHHG, the comparison of all three spectra highlight the unique physics inherent to BHHG as compared to single-color linear HHG, in particular the propensity rules that govern the relative intensity of LCP and RCP harmonic peaks [42]. First, we note that in Ar the intensity of RCP harmonics is higher than those of LCP harmonics until ~50 eV, which corresponds to the Cooper minimum (discussed further below). This preference for harmonics co-rotating with the NIR driver is a result of the higher intensity of the NIR component of the bicircular field, and can be used as a control parameter to tailor the ellipticity of the underlying attosecond pulse trains [42,43]. In Ne; however, the opposite is observed; intensities of RCP harmonics are lower than those of LCP harmonics (except near the cutoff) despite the higher intensity of the NIR field. The difference in Ar and Ne is due to the differing phases and amplitudes of the recombination dipole matrix elements, which tend to favor harmonics that rotate with the lower-frequency driver in Ne, as also observed in Ref. [42]. Finally, in He we observe a similar intensity of RCP and LCP harmonic orders, which is

Optics EXPRESS

due to the electrons being ionized from an initial *s* state and thus leads to similar amplitudes for the recombination matrix elements, and thus similar RCP and LCP harmonic intensities.

3.2. Bright, single-helicity high harmonics covering M-absorption edges of ferromagnetic materials

One of the more striking features of the HHG spectrum in Ar driven by 0.8 μm + 2.0 μm fields is the sharp reversal of the spectral intensities of RCP and LCP harmonics at photon energies around ~50 eV, corresponding to the Cooper minimum in Ar (Figs. 1(a) and 2(a)). This Cooper minimum-induced helicity reversion in Ar was observed in Ref. [45,47], and is attributed to the different amplitudes and phases of the transition dipole matrix elements for electron recombination from laser-dressed continuum states. Destructive interference in the vicinity of the Cooper minimum typically results in a characteristic spectral dip in the HHG spectra [45,47,57,58,59]. However, unlike previous studies, we do not observe a decrease of the overall HHG yield near the Cooper minimum (aside from a slight decrease in LCP harmonic intensity near 45 eV, also observed in Ref. [42]). Instead, we observe a smooth variation of the HHG intensities across the entire harmonic envelope—the harmonic peaks remain discrete, while also retaining their spectral width (Figs. 1(b),2(a)). This absence of a dip could be the result of the concerted effects of phase matching [5,7,59] in the hollow core capillary and the exact parameters of the bicircular field [60]. This unique characteristic allows us to actively reshape the spectrum, by driving the HHG process at high pressure. In this case, we observe an intensity reversal and near complete suppression of RCP harmonics beyond the Cooper minimum, resulting in a high-energy spectrum consisting of harmonics of a single helicity. The presence of a single helicity supports a train of circularly polarized attosecond pulses, which can be obtained by filtering for the near cutoff harmonics. Finally, we note that the single helicity portion of the HHG spectrum in Fig. 2(b) naturally coincides with the *M* absorption edges of 3*d* transition-metal ferromagnets (e.g., Fe, Co, and Ni).

3.3. Comparison of BHHG and linearly polarized HHG cutoffs and extension of BHHG cutoffs into the "water window"

In order to explore the photon energy limits to which bright, phase matched, circularly-polarized HHG can extend, we experimentally determined the high-energy harmonic cutoff in Ar, Ne, and He employing either 1.3 or 2.0 μm as the MIR component of the bicircular field. To date, the observed cutoffs lie somewhere between the linearly polarized cutoffs of the constituent laser fields. However, a rigorous experimental study is still lacking. To explore the cutoffs for combined NIR-MIR driving lasers, we first optimize the HHG spectrum for suppression of spin-forbidden peaks and for brightness. We then change the helicity of one laser to linear and record the experimental cutoff for each beam in the bicircular field without changing the pulse energy in the beam. As expected, we find that the experimental HHG cutoffs lie between the cutoffs obtained for the linearly polarized fields (Fig. 3(a)).

To further probe the photon energy limits for bright circular HHG, we employ theoretical simulations to show that by using a combination of counter-rotating MIR lasers, the HHG spectra can extend into the water window region, beyond the carbon *K* edge (Figs. 3(b)-(d)). Moreover, the lower photon energies of MIR drivers lead to a much higher spectral density of the emitted harmonics. This can enable chiral spectroscopies and imaging of organic compounds with a higher spectral resolution than in previous studies employing circularly polarized HHG sources for chiral spectroscopies and imaging. High-pulse energy MIR sources based on optical parametric chirped pulse amplification (OPCPA) technology, along with advances in MIR polarization optics, can thus be used produce bright, circularly-polarized SXR light.

The use of non-commensurate NIR-MIR bicircular fields thus has the clear advantages of accessing higher HHG photon energies and higher spectral density; however, there are practical

Optics EXPRESS

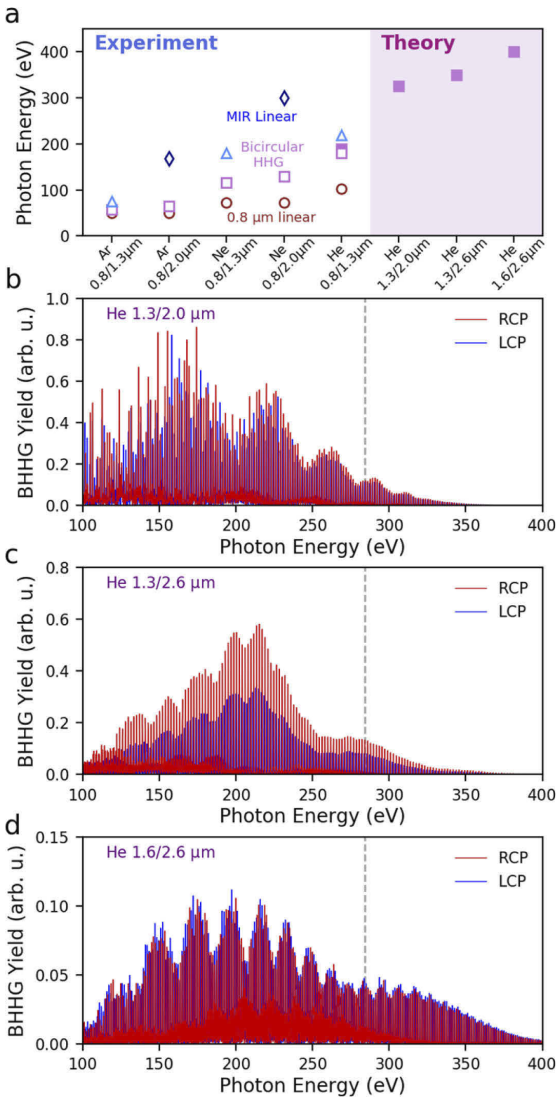

Fig. 2. (a) Comparison of the experimental (open symbols) and theoretical (filled symbols) circularly polarized HHG cutoffs for a NIR-MIR bicircular driving field (open squares), as well as the linearly polarized cutoffs for each laser wavelength (open diamonds 2μm, open triangles 1.3μm, open circles 0.8μm). The theoretical cutoffs for the MIR-MIR bicircular field extend beyond the carbon *K* edge, well into the water window of the SXR region. (b-d). Theoretical HHG spectra obtained in He with a MIR-MIR bicircular fields, exhibiting a dense spectrum spanning the carbon *K* absorption edge (dashed-gray line).

aspects that must be considered when constructing a bicircular field with a MIR component for bicircular HHG. For instance, the spectral density increases with increasing the wavelength of the MIR component, because the separation between adjacent harmonics in each doublet decreases. Additionally, harmonic peaks arising from channels where an additional photon of the "wrong" polarization is absorbed can appear very close to the main right and left circularly polarized harmonic doublets [32], and suppressing these harmonic peaks requires sufficient spectral resolution so that they can be discerned from the main doublets. This places strict demands

Optics EXPRESS

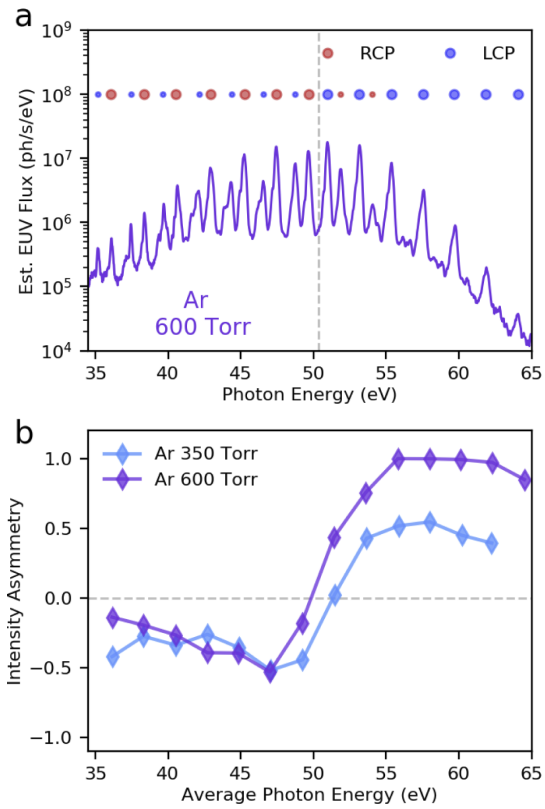

Fig. 3. (a) High-pressure circularly-polarized HHG spectrum in Ar, exhibiting a complete suppression of right circularly polarized harmonic orders just beyond the Cooper minimum (dashed grey line). (b) Intensity asymmetry ($A = (I_{LCP} - I_{RCP})/(I_{LCP} + I_{RCP})$) of each harmonic doublet in (a), at different pressures.

on the accuracy of waveplates and the spectral resolution of the spectrometer. Additionally, MIR drivers require higher pressures for proper phase matching as compared to NIR laser fields, which requires optimized geometries and vacuum systems to obtain bright, high-energy spectra. Despite these technological challenges, schemes employing MIR components for driving BHHG should be highly successful for producing coherent, circularly polarized SXR radiation into the water window and potentially to the L absorption edges of magnetic materials containing 3d transition metals.

4. Conclusion

In summary, we have experimentally and theoretically demonstrated the unique advantages of employing an optimized phase matching geometry coupled with bicircular fields possessing MIR components for producing high energy, highly elliptically polarized high harmonics. Such a combination has allowed us, for the first time, to generate a high-harmonic spectrum consisting of a single helicity without the need of additional optics or beamline components. This unique spectrum should also stimulate additional theoretical investigations into the quantum dynamics of Cooper minimum-induced phenomena in HHG. We have also shown that high-energy spectra obtained in He span the N absorption edges of 4f rare-earth ferromagnetic elements, which provides for a bright, tabletop source for studying spin dynamics in emerging spintronic devices

Optics EXPRESS

and materials. Additionally, we have utilized these results to provide a roadmap for scaling of photon energies in BHHG, and shown via advanced theoretical simulations that circularly polarized SXR harmonics can be generated that span the carbon *K* edge. As such, these results not only provide for unique tabletop sources of highly elliptically polarized EUV and SXR light, but should also stimulate the development of MIR bicircular schemes for producing high harmonic spectra beyond the water window that reach the *L* absorption edges of 3d transition metals.

Funding. Department of Energy BES (DE-FG02-99ER14982); Air Force Office of Scientific Research (FA9550-16-1-0121); National Science Foundation (DGE-1144083, DGE-1650115); European Research Council (8511201); Ministerio de Ciencia, Innovación y Universidades (PID2019-106910GB-100); Junta de Castilla y León (SA287P18); Ramón y Cajal contract (RYC-2017-22745).

Acknowledgements. The experimental research was done at JILA. M. M. M and H. C. K acknowledge support from Department of Energy BES and AFOSR MURI awards for the NIR and MIR light science research, respectively. J. L. E., N. B., and Q. L. D. N. acknowledge support from National Science Foundation Graduate Research Fellowships. G. H.-G. acknowledges support from European Research Council (ERC) under the European Union's Horizon 2020 research and innovation programme (grant agreement No. 851201), Ministerio de Ciencia e Innovacíon y Universidades for a Ramón y Cajal contract, co-funded by the European Social Fund.

Disclosures. H.K.: KMLabs Inc. (I, E, P). M. M.: KMLabs Inc. (I, P). Other authors declare no conflicts of interest.

Data Availability. The data presented in this manuscript are not publicly available at this time but may be obtained from the authors upon reasonable request.

References

1. A. McPherson, G. Gibson, H. Jara, U. Johann, T. S. Luk, I. A. McIntyre, K. Boyer, and C. K. Rhodes, "Studies of multiphoton production of vacuum-ultraviolet radiation in the rare gases," J. Opt. Soc. Am. **4**(4), 595 (1987)..
2. M. Ferray, A. L'Huillier, X. F. Li, L. A. Compre, G. Mainfry, and C. Manus, "Multiple-harmonic conversion of 1988 nm radiation in rare gases," J. Phys. B: At. Mol. Opt. Phys. **21**(3), L31–L35 (1988).
3. J. L. Krause, K. J. Schafer, and K. C. Kulander, "High-order harmonic generation from atoms and ions in the high intensity regime," Phys. Rev. Lett. **68**(24), 3535–3538 (1992).
4. T. Popmintchev, M. C. Chen, D. Popmintchev, P. Arpin, S. Brown, S. Alisauskas, G. Andriukaitis, T. Balciunas, O. D. Mucke, A. Pugzlys, A. Baltuska, B. Shim, S. E. Schrauth, A. Gaeta, C. Hernández-García, L. Plaja, A. Becker, A. Jaron-Becker, M. M. Murnane, and H. C. Kapteyn, "Bright coherent ultrahigh harmonics in the keV X-ray regime from mid-infrared femtosecond lasers," Science **336**(6086), 1287–1291 (2012)..
5. A. Rundquist, C. G. Durfee, Z. Chang, C. Herne, S. Backus, M. M. Murnane, and H. C. Kapteyn, "Phase-matched generation of coherent soft X-rays," Science **580**(5368), 1412 (1998)..
6. H. C. Kapteyn, M. M. Murnane, and I. P. Christov, "Extreme nonlinear optics: Coherent X rays from lasers," *invited article*, *Phys. Today*, 58(3), 39–46 (2005).
7. T. Popmintchev, M.-C. Chen, A. Bahabad, M. Gerrity, P. Sidorenko, O. Cohen, I. P. Christov, M. M. Murnane, and H. C. Kapteyn, "Phase matching of high harmonic generation in the soft and hard X-ray regions of the spectrum," Proceedings of the National Academy of Sciences **106**(26), 10516–10521 (2009).
8. V. Tosa, H. T. Kim, I. J. Kim, and C. H. Nam, "High-order harmonic generation by chirped and self-guided femtosecond laser pulses. II. Time-frequency analysis," Phys. Rev. A **71**(6), 063808 (2005).
9. C. Altucci, R. Bruzzese, C. de Lisio, M. Nisoli, E. Priori, S. Stagira, M. Pascolini, L. Poletto, P. Villoresi, V. Tosa, and K. Midorikawa, "Phase-matching analysis of high-order harmonics generated by truncated Bessel beams in the sub-10-fs regime," Phys. Rev. A **68**(3), 033806 (2003).
10. R. A. Bartels, A. Paul, H. Green, H. C. Kapteyn, M. M. Murnane, S. Backus, I. P. Christov, Y. Liu, D. Attwood, and C. Jacobsen, "Generation of spatially coherent light at extreme ultraviolet wavelengths," Science **297**(5580), 376–378 (2002).
11. M. C. Chen, P. Arpin, T. Popmintchev, M. Gerrity, B. Zhang, M. Seaberg, M. M. Murnane, and H. C. Kapteyn, "Bright, Coherent, Ultrafast Soft X-Ray Harmonics Spanning the Water Window from a Tabletop Source," Phys. Rev. Lett. **105**(17), 173901 (2010).
12. I. P. Christov, M. M. Murnane, and H. C. Kapteyn, "High-harmonic generation of attosecond pulses in the "single-cycle" regime," Phys. Rev. Lett. **78**(7), 1251–1254 (1997).
13. M. C. Chen, C. Hernández-García, C. Mancuso, F. Dollar, B. Galloway, D. Popmintchev, P. C. Huang, B. Walker, L. Plaja, A. Jaron-Becker, A. Becker, T. Popmintchev, M. M. Murnane, and H. C. Kapteyn, "Generation of bright isolated attosecond soft X-ray pulses driven by multi-cycle mid-infrared lasers," Proceedings of the National Academy of Sciences **111**(23), E2361–E2367 (2014).
14. G. Sansone, E. Benedetti, F. Calegari, C. Vozzi, L. Avaldi, R. Flammini, L. Poletto, P. Villoresi, C. Altucci, R. Velotta, S. Stagira, S. De Silverstri, and M. Nisoli, "Isolated single-cycle attosecond pulses," Science **314**(5798), 443–446 (2006).

Optics EXPRESS

15. E. Gouliemakis, M. Schultze, M. Hofstetter, V. S. Yakovlev, J. Gagno, M. Uiberacker, A. L. Aquila, E. M. Gullikson, D. T. Attwood, R. Kienberger, F. Krausz, and U. Kleineberg, "Single-cycle nonlinear optics," Science **320**(5883), 1614–1617 (2008).
16. Z. Tao, C. Chen, T. Szilvasi, M. Keller, M. Mavrikakis, H. Kapteyn, and M. Murnane, "Direct time-domain observation of attosecond final-state lifetimes in photoemission from solids," Science **353**(6294), 62–67 (2016).
17. P. Tengdin, C. Gentry, A. Blonksy, D. Zusin, M. Gerrity, L. Hellbrück, M. Hofherr, J. Shaw, Y. Kvashnin, E. K. Delczeg-Czirjak, M. Arora, H. Nembach, T. J. Silva, S. Mathias, M. Aeschlimann, H. C. Kapteyn, D. Thonig, K. Koumpouras, O. Eriksson, and M. M. Murnane, "Direct light-induced spin transfer between different elements in a spintronic Heusler material via femtosecond laser excitation," Sci. Adv. **6**, eaaz1100 (2020).
18. X. Shi, W. You, Y. Zhang, Z. Tao, P. M. Oppeneer, X. Wu, R. Thomale, K. Rossnagel, M. Bauer, H. Kapteyn, and M. Murnane, "Ultrafast electron calorimetry uncovers a new long-lived metastable state in 1*T*-$TaSe_2$ mediated by mode-selective electron-phonon coupling," Sci. Adv. **5**, eaav4449 (2019).
19. Y. C. Zhang, X. Shi, W. J. You, Z. S. Tao, Y. G. Zhong, F. C. Kabeer, P. Maldonado, P. M. Oppeneer, M. Bauer, K. Rossnagel, H. Kapteyn, and M. Murnane, "Coherent modulation of the electron temperature and electron-phonon couplings in a 2D material," Proc Natl Acad Sci USA **117**(16), 8788–8793 (2020).
20. F. Calegari, D. Ayuso, A. Trabattoni, L. Belshaw, S. De Camillis, S. Anumela, F. Frassetto, L. Poletto, A. Palacios, P. Decleva, J. B. Greenwood, F. Martín, and M. Nisoli, "Ultrafast electron dynamics in phenylalanine initiated by attosecond pulses," Science **346**(6207), 336 (2014).
21. K. Hoogebom-Pot, J. N. Hernandez-Charpak, X. Gu, T. D. Frazer, E. H. Anderson, W. Chao, R. W. Falcone, R. Yang, M. M. Murnane, H. C. Kapteyn, and D. Nardi, "A new regime of nanoscale thermal transport: Collective diffusion increases dissipation efficiency," Proc Natl Acad Sci USA **112**(16), 4846–4851 (2015).
22. D. F. Gardner, M. Tanksalvala, E. R. Shanblatt, X. Zhang, B. R. Galloway, C. L. Porter, R. Karl, C. Bevis, D. E. Adams, H. C. Kapteyn, M. M. Murnane, and G. F. Mancini, "Subwavelength coherent imaging of periodic samples using a 13.5 nm tabletop high-harmonic light source," Nature Photon **11**(4), 259–263 (2017).
23. O. Kfir, S. Zayko, C. Nolte, M. Sivis, M. Möller, B. Hebler, S. S. Phani, K. Arekapudi, D. Steil, S. Schäfer, M. Albrecht, O. Cohen, S. Mathais, and C. Ropers, "Nanoscale magnetic imaging using circularly polarized high-harmonic radiation," Sci. Adv. **3**, eaao4641 (2017).
24. R. M. Karl, G. F. Mancini, J. L. Knobloch, T. D. Frazer, J. N. Hernandez-Charpak, B. Abad, D. F. Gardner, E. R. Shanblatt, M. Tanksalvala, C. L. Porter, C. S. Bevis, D. E. Adams, H. C. Kapteyn, and M. M. Murnane, "Full-field imaging of thermal and acoustic dynamics in an individual nanostructure using tabletop high harmonic beams," Sci. Adv. **4**, eaau4295 (2018).
25. M. Tanksalvala, C. L. Porter, Y. Esashi, B. Wang, N. W. Jenkins, Z. Zhang, G. P. Miley, J. L. Knobloch, B. McBennett, N. Horiguchi, S. Yazdi, J. Zhou, M. W. Jacobs, C. S. Bevis, R. M. Karl, P. Johnsen, D. Ren, L. Waller, D. E. Adams, S. L. Cousin, C.-T. Liao, J. Miao, M. Gerrity, H. C. Kapteyn, and M. M. Murnane, "Nondestructive, high-resolution, chemically specific 3D nanostructure characterization using phase-sensitive EUV imaging reflectometry," Sci. Adv. **7**(5), eabd9667 (2021).
26. T. D. Frazer, J. L Knobloch, J. N. Hernández-Charpak, K. M. Hoogeboom-Pot, D. Nardi, S. Yazdi, W. Chao, E. H. Anderson, M. K. Tripp, S. W. King, H. C. Kapteyn, M. M. Murnane, and B. Abad, "Full characterization of ultrathin 5-nm low-κ dielectric bilayers: Influence of dopants and surfaces on the mechanical properties," Phys. Rev. Materials **4**(7), 073603 (2020).
27. P. B. Corkum, "Plasma perspective on strong field multiphoton ionization," Phys. Rev. Lett. **71**(13), 1994–1997 (1993).
28. M. Lewenstein, Ph. Balcou, M. Yu Ivanov, A. L'Huillier, and P. B. Corkum, "Theory of high-harmonic generation by low frequency laser fields," Phys. Rev. A **49**(3), 2117–2132 (1994).
29. R. Bartels, S. Backus, E. Zeek, L. Misoguti, G. Vdovin, I. P. Christov, M. M. Murnane, and H. C. Kapteyn, "Shaped-pulse optimisation of coherent soft-x-rays," Nature **406**(6792), 164–166 (2000).
30. R. Zerne, C. Altucci, M. Bellini, M. B. Gaarde, T. W. Hänsch, A. L'Huillier, C. Lyngå, and C.-G. Wahlström, "Phase-locked high-order harmonic sources," Phys. Rev. Lett. **79**(6), 1006–1009 (1997).
31. O. Kfir, P. Grychtol, E. Turgut, R. Knut, D. Zusin, D. Popmintchev, T. Popmintchev, H. Nembach, J. M. Shaw, A. Fleischer, H. Kapteyn, M. Murnane, and O. Cohen, "Generation of bright phase-matched circularly-polarized extreme ultraviolet high harmonics," Nature Photon **9**(2), 99–105 (2015).
32. T. Fan, P. Grychtol, R. Knut, C. Hernández-García, D. D. Hickstein, D. Zusin, C. Gentry, F. J. Dollar, C. A. Mancuso, C. W. Hogle, O. Kfir, D. Legut, K. Carva, J. L. Ellis, K. M. Dorney, C. Chen, O. G. Shpyrko, E. E. Fullerton, O. Cohen, P. M. Oppeneer, D. B. Milošević, A. Becker, A. A. Jaroń-Becker, T. Popmintchev, M. M. Murnane, and H. C. Kapteyn, "Bright circularly polarized soft x-ray high harmonics for X-ray magnetic circular dichroism," Proc Natl Acad Sci USA **112**(46), 14206–14211 (2015).
33. D. D. Hickstein, F. J. Dollar, P. Grychtol, J. Ellis, R. Knut, C. Hernández-García, D. Zusin, C. Gentry, J. Shaw, T. Fan, K. Dorney, A. Becker, A. Jaroń-Becker, H. C. Kapteyn, and M. M. Murnane, "Non-collinear generation of angularly isolated circularly polarized high harmonics," Nature Photon **9**(11), 743–750 (2015).
34. P-C. Huang, C. Hernández-García, J.-T. Huang, P-Y. Huang, C.-H. Lu, L. Rego, D. D. Hickstein, J. L. Ellis, A. Jaron-Becker, A. Becker, S.-D. Yang, C. G. Durfee, L. Plaja, H. C. Kapteyn, M. M. Murnane, A. H. Kung, and M.-C. Chen, "Polarization control of isolated high-harmonic pulses," Nature Photon **12**(6), 349–354 (2018).

Optics EXPRESS

35. K. M. Dorney, L. Rego, N. J. Brooks, J. San Román, C.-T. Liao, J. L. Ellis, D. Zusin, C. Gentry, Q. L. Nguyen, J. M. Shaw, A. Picón, L. Plaja, H. C. Kapteyn, M. M. Murnane, and C. Hernández-García, "Controlling the polarization and vortex charge of attosecond high-harmonic beams via simultaneous spin-orbit momentum conservation," Nature Photon **13**(2), 123–130 (2019).
36. L. Rego, K. M. Dorney, N. J. Brooks, Q. L. Nguyen, C.-T. Laio, J. San Román, D. E. Couch, A. Liu, E. Pisanty, M. Lewenstein, L. Plaja, H. C. Kapteyn, M. M. Murnane, and C. Hernández-García, "Generation of extreme-ultraviolet beams with time-varying orbital angular momentum," Science **364**(6447), eaaw9486 (2019).
37. F. Kong, C. Zhang, H. Larocque, F. Bouchard, Z. Li, M. Taucher, G. Brown, S. Severino, T. J. Hammond, E. Karimi, and P. B. Corkum, "Spin-constrained orbital angular-momentum control in high-harmonic generation," Phys. Rev. Research **1**(3), 032008 (2019).
38. M. Chini, K. Zhao, and Z. Chang, "The generation, characterization and applications of broadband isolated attosecond pulses," Nature Photon **8**(3), 178–186 (2014).
39. H. Eichmann, A. Egbert, S. Nolte, C. Momma, B. Wellegehausen, W. becker, S. Long, and J. K. McIver, "Polarization-dependent high-order two-color mixing," Phys. Rev. A **51**(5), R3414–R3417 (1995).
40. S. Long, W. Becker, and J. K. McIver, "Model calculations of polarization-dependent two-color high-harmonic generation," Phys. Rev. A **52**(3), 2262–2278 (1995).
41. A. Fleischer, O. Kfir, T. Diskin, P. Sidorenko, and O. Cohen, "Spin angular momentum and tunable polarization in high-harmonic generation," Nature Photon **8**(7), 543–549 (2014).
42. K. M. Dorney, J. L. Ellis, C. Hernández-García, D. D. Hickstein, C. A. Mancuso, N. Brooks, T. Fan, G. Fan, D. Zusin, C. Gentry, P. Grychtol, H. C. Kapteyn, and M. M. Murnane, "Helicity-selective enhancement and polarization control of attosecond high harmonic waveforms driven by bichromatic circularly polarized laser fields," Phys. Rev. Lett. **119**(6), 063201 (2017).
43. Á. Jiménez-Galán, N. Zhavoronkov, D. Ayuso, F. Morales, S. Patchkovskii, M. Schloz, E. Pisanty, O. Smirnova, and M. Ivanov, "Control of attosecond light polarization in two-color bicircular fields," Phys. Rev. A **97**(2), 023409 (2018).
44. D. Baykusheva, M. S. Ahsan, N. Lin, and H. J. Wörner, "Bicircular high-harmonic spectroscopy reveals dynamical symmetries of atoms and molecules," Phys. Rev. Lett. **116**(12), 123001 (2016).
45. D. Baykusheva, S. Brennecke, M. Lien, and H. J. Wörner, "Signatures of electronic structure in bicircular high-harmonic generation," Phys. Rev. Lett. **119**(20), 203201 (2017).
46. D. Baykusheva and H. J. Wörner, "Chiral discrimination through bielliptical high-harmonic spectroscopy," Phys. Rev. X **8**(3), 031060 (2018).
47. D. B. Milošević, "Low-frequency approximation for high-order harmonic generation by a bicircular laser field," Phys. Rev. A **97**(1), 013416 (2018).
48. C. Ding, W. Xiong, T. Fan, D. D. Hickstein, T. Popmintchev, X. Zhang, M. Walls, M. M. Murnane, and H. C. Kapteyn, "High flux coherent super-continuum soft X-ray source driven by a single-stage, 10mJ, Ti:sapphire amplifier-pumped OPA," Opt. Express **22**(5), 6194 (2014).
49. F. H. M. Faisal, "Multiple absorption of laser photons by atoms," J. Phys. B: At. Mol. Phys. **6**(4), L89–L92 (1973).
50. H. R. Reiss, "Effect of an intense electromagnetic field on a weakly bound system," Phys. Rev. A **22**(5), 1786–1813 (1980).
51. W. Becker, A. Lohr, M. Kleber, and M. Lewenstein, "A unified theory of high-harmonic generation: Application to polarization properties of the harmonics," Phys. Rev. A **56**(1), 645–656 (1997).
52. J. A. Pérez-Hernández, L. Roso, and L. Plaja, "Harmonic generation beyond the Strong-Field Approximation: the physics behind the short-wave-infrared scaling laws," Opt. Express **17**(12), 9891 (2009).
53. J. A. Pérez-Hernández and L. Plaja, "Quantum description of the high-order harmonic generation in multiphoton and tunneling regimes," Phys. Rev. A **76**(2), 023829 (2007).
54. E. Pisanty and Á. Jiménez-Galán, "Strong-field approximation in a rotating frame: High-order harmonic emission from *p* states in bicircular fields," Phys. Rev. A **96**(6), 063401 (2017).
55. O. E. Alon, V. Averbukh, and N. Moiseyev, "Selection rules for the high harmonic generation spectra," Phys. Rev. Lett. **80**(17), 3743–3746 (1998).
56. O. Kfir, P. Grychtol, E. Turgat, R. Knut, D. Zusin, A. Fleischer, E. Bordo, T. Fan, D. Popmintchev, T. Popmintchev, H. Kapteyn, M. Murnane, and O. Cohen, "Helicity-selective phase-matching and quasi-phase matching of circularly polarized high-order harmonics: towards chiral attosecond pulses," J. Phys. B: At. Mol. Opt. Phys. **49**(12), 123501 (2016).
57. H. J. Wörner, H. Niikura, J. B. Bertrand, P. B. Corkum, and D. M. Villeneuve, "Observation of electronic structure minima in high-harmonic generation," Phys. Rev. Lett. **102**(10), 103901 (2009).
58. C. Jin, A.-T. Le, and C. D. Lin, "Medium propagation effects in high-order harmonic generation of Ar and N_2," Phys. Rev. A **83**(2), 023411 (2011).
59. J. P. Farrell, L. S. Spector, B. K. McFarland, P. H. Bucksbaum, M. Gühr, M. B. Gaarde, and K. J. Schafer, "Influence of phase matching on the Cooper minimum in Ar in high-order harmonic spectra," Phys. Rev. A **83**(2), 023420 (2011).
60. G. S. Boltaev, R. A. Ganeev, N. A. Abbasi, M. Iqbal, V. V. Kim, H. Al-Harmi, X. M. Tong, and A. S. Alnaser, "Routes to control Cooper minimum in high order harmonics generated in argon gas," New J. Phys. **22**(8), 083031 (2020).